REPORT DOCUMENTATION PAGE

Form Approved
OMB No. 0704-0188

1. REPORT DATE *(DD-MM-YYYY)*	**2. REPORT TYPE**	**3. DATES COVERED** *(From - To)*
22-05-2006	Technical Paper	

4. TITLE AND SUBTITLE

Comparison of Numerical and Experimental Near-Field Plasma Properties of the BHT-200-X3 Hall Thruster (Preprint)

5a. CONTRACT NUMBER

5b. GRANT NUMBER

5c. PROGRAM ELEMENT NUMBER

6. AUTHOR(S)
Garrett D. Reed (ERC); William A. Hargus & Douglas B. VanGilder (AFRL/PRSS)

5d. PROJECT NUMBER
23080535

5e. TASK NUMBER

5f. WORK UNIT NUMBER

7. PERFORMING ORGANIZATION NAME(S) AND ADDRESS(ES)

Air Force Research Laboratory (AFMC)
AFRL/PRSS
1 Ara Drive
Edwards AFB CA 93524-7013

8. PERFORMING ORGANIZATION REPORT NUMBER

AFRL-PR-ED-TP-2006-157

9. SPONSORING / MONITORING AGENCY NAME(S) AND ADDRESS(ES)

Air Force Research Laboratory (AFMC)
AFRL/PRS
5 Pollux Drive
Edwards AFB CA 93524-70448

10. SPONSOR/MONITOR'S ACRONYM(S)

11. SPONSOR/MONITOR'S NUMBER(S)
AFRL-PR-ED-TP-2006-157

12. DISTRIBUTION / AVAILABILITY STATEMENT

Approved for public release; distribution unlimited (AFRL-ERS-PAS-2006-113)

13. SUPPLEMENTARY NOTES
Presented at the 42nd AIAA/ASME/SAE/ASEE Joint Propulsion Conference, Sacramento, CA, 9-12 July 2006.

14. ABSTRACT

Near-field ion velocity distributions of a BusekBHT-200-X3 xenon Hall thruster obtained through numerical simulation are compared with laser-induced fluorescence measurements taken for one nominal operating condition. The numerical code Hybrid-PIC Hall, a 2D hybrid particle-in-cell model, is used to simulate an axisymmetric cross section of the plasma acceleration zone. A set of nine HP Hall simulations are run using three different cathode positions and Bohm electron mobility coefficients to study the effects of these parameters on ion acceleration. Six additional cases were run in an attempt to better match the simulation results to the experimental data. For model validation, agreement between the numerical and experimental results is examined. The results show that it is difficult to match both the global operational parameters (i.e, thrust, discharge current, and beam current) and the ion velocity distributions. The shape of the axial velocity distributions can be closely matched by using high Bohm electron mobility values. However, this correlation comes at the expense of peak ion velocity and discharge current agreement. Radial velocity distributions are more closely matched by the simulations, but the simulations uniformly predict lower than measured inward and higher than measured outward radial velocity components (relative to the centerline) from the annular acceleration channel.

15. SUBJECT TERMS

16. SECURITY CLASSIFICATION OF:			**17. LIMITATION OF ABSTRACT**	**18. NUMBER OF PAGES**	**19a. NAME OF RESPONSIBLE PERSON**
					Dr. William A. Hargus
a. REPORT	**b. ABSTRACT**	**c. THIS PAGE**	A	25	**19b. TELEPHONE NUMBER** *(include area code)*
Unclassified	**Unclassified**	**Unclassified**			N/A

Standard Form 298 (Rev. 8-98)
Prescribed by ANSI Std. 239.18

Comparison of Numerical and Experimental Near-Field Plasma Properties of the BHT-200-X3 Hall Thruster

Michael R. Nakles*
ERC, Inc., Edwards Air Force Base, CA, 93524

William A. Hargus, Jr.† and Douglas B. VanGilder†
Air Force Research Laboratory, Edwards Air Force Base, CA, 93524

Near-field ion velocity distributions of a Busek BHT-200-X3 xenon Hall thruster obtained through numerical simulation are compared with laser-induced fluorescence measurements taken for one nominal operating condition. The numerical code Hybrid-PIC Hall, a 2D hybrid particle-in-cell model, is used to simulate an axisymmetric cross section of the plasma acceleration zone. A set of nine HPHall simulations are run using three different cathode positions and Bohm electron mobility coefficients to study the effects of these parameters on ion acceleration. Six additional cases were run in an attempt to better match the simulation results to the experimental data. For model validation, agreement between the numerical and experimental results is examined. The results show that it is difficult to match both the global operational parameters (i.e. thrust, discharge current, and beam current) and the ion velocity distributions. The shape of the axial velocity distributions can be closely matched by using high Bohm electron mobility values. However, this correlation comes at the expense of peak ion velocity and discharge current agreement. Radial velocity distributions are more closely matched by the simulations, but the simulations uniformly predict lower than measured inward and higher than measured outward radial velocity components (relative to the centerline) from the annular acceleration channel.

I. Introduction

Numerical simulation is an attractive option to study Hall thruster near-plume plasma properties. Simulations can potentially be faster and less costly than running experiments. However, currently available numerical models first require validation through correlation with experimental results before they can be considered a dependable method for predicting Hall thruster properties. One Hall thruster code that models the plasma in the acceleration channel and near-plume is Hybrid-PIC Hall (HPHall) developed by Fife.[1] It is a 2D particle-in-cell model, which simulates an axisymmetric cross section of the plasma acceleration zone of a Hall thruster with a user-defined geometry.

The objective of this study is to compare numerical HPHall results to experimental data in order to evaluate the ability of HPHall to predict the near-plume plasma properties of a Hall thruster. Previously, studies of this nature have been primarily based on bulk ion velocity comparisons. Ideally, ion velocity comparisons reveal the correlation between the acceleration mechanisms of the actual thruster and the model. Ion velocity distribution functions (VDF's) provide insight about the size and location of the ionization region and the ion collisionality.

One method for measuring ion velocity experimentally is laser-induced fluorescence (LIF).[2] This technique is especially well suited for near-plume measurements because it is non-intrusive. Furthermore, LIF can also provide velocity distribution information in specific instances.

*Research Engineer, AFRL/PRSS, 1 Ara Rd. Edwards AFB, CA 93524, Member AIAA
†Research Engineer, AFRL/PRSS, 1 Ara Rd. Edwards AFB, CA 93524, Senior Member AIAA

The 200 W Busek BHT-200-X3[3] thruster serves as the subject for this comparison study between HPHall simulations and experimental LIF data. A model of the thruster was created in HPHall and several simulations were run with various input parameters. Experimental LIF data from Hargus and Charles[4] was compared with the modeling data to evaluate the accuracy of HPHall near-plume ion velocity predictions.

The long term goal of this effort is to create an accurate model of the internal plasma parameters of the BHT-200-X3 Hall thruster. Once this is accomplished, it should be possible to predict the lifetime of a thruster solely via simulation. Ideally, this capability may then be applied to other thrusters.

II. HPHall Model

HPHall is a hybrid particle-in-cell (PIC) model of an axisymmetric cross section of the plasma acceleration zone inside a Hall thruster. Heavy particle motion is implemented using a PIC methodology involving a particle-tracking Boltzmann solver. Electrons are modeled as a quasi-one-dimensional fluid[1] using three equations. The code solves a time accurate electron energy equation for the electron temperature and determines the electric field strength from a generalized Ohm's law. A current conservation equation is also solved. The model operates under the assumptions of a static magnetic field, quasineutrality, Maxwellian electrons, and a combination of Bohm and classical diffusion across magnetic field lines. A Monte Carlo collision process is used to create ions in the acceleration channel.

HPHall requires a user-defined 2D grid for the simulation domain that contains the thruster acceleration channel and the near-field plume region. The non-uniform spatial grid used for the BHT-200-X3 is shown in Fig. 1. The code solves for plasma properties such as potential, particle densities, and temperatures on the 2D grid during the simulation. HPHall also requires the magnetic field at each grid point as input. The 2D magnetic field for the thruster was solved using Maxwell SV®[5] software. Agreement between measurements and magnetic field predictions from Maxwell indicated that accurate magnetic field values were used in the HPHall simulations.

HPHall assumes the curl of the thruster's magnetic field is negligible and thus allows for the existence of a magnetic stream function, λ, whose gradient is everywhere orthogonal to the magnetic field.[1] HPHall further assumes that electron temperature is constant along magnetic field stream lines. From these assumptions, a constant thermalized plasma potential, $\phi^*(\lambda)$, exists along magnetic field lines. Plasma potential is calculated along magnetic field lines as

$$\phi - \frac{kT_e}{e}\ln(n_e) = \phi^*(\lambda) \tag{1}$$

where k is the Boltzmann constant, T_e is electron temperature, and n_e is electron density. Therefore, plasma potential is only a function of electron density along magnetic field lines.

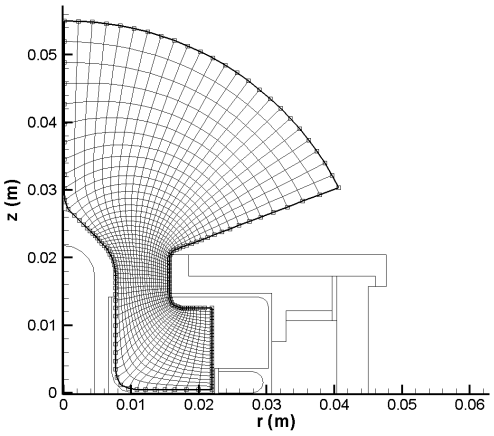

Figure 1. BHT-200-X3 simulation grid shown within the thruster geometry.

The quasi-one-dimensional equations are solved only between the anode and cathode boundaries. Cathode and anode boundaries are set along magnetic streamlines. A Dirichlet boundary condition is placed at the cathode which sets the electron temperature to 5 eV (a value based on experimental measurements).[1] Downstream of the cathode, linear interpolation is used to calculate T_e and ϕ^*. Although the cathode boundary condition should ideally correspond to the magnetic field line that intersects the actual cathode location, the cathode boundary condition can be varied in order to change the potential field of the acceleration channel.

Another method of changing ion behavior in the acceleration channel is adjusting the electron cross-field mobility. Electron cross-field mobility in HPHall is calculated using both classical and Bohm diffusion terms because neither the classical nor Bohm model alone can appropriately represent the mobility measured experimentally in Hall thrusters.[1] The cross-field mobility is modeled as

$$\mu_{e,\perp} = \frac{\mu_e}{{\beta_e}^2} + K_B\frac{1}{16B} \tag{2}$$

where μ_e is the electron mobility in the weakly ionized limit, $\mu_{e,\perp}$ is the electron conductivity normal to

magnetic field lines, β_e is the electron Hall parameter, and B is the magnetic field strength. The first term on the right hand side is the classical electron mobility term ($\sim 1/B^2$), where electrons rely on collisions with heavy particles to traverse magnetic field lines. It is inversely proportional to the square of the magnetic field strength. The second term on the right hand side is the semi-empirical Bohm mobility term, which accounts for plasma turbulence providing enhanced cross-field electron mobility ($\sim 1/B$). The 1/16 constant represents the maximum observed value for Bohm cross-field diffusion. The empirical coefficient K_B may be adjusted between 0 and 1 to account for the effective plasma turbulence.[6] Fife determined that for the SPT-70 Hall thruster, 0.15 was the optimal choice for matching thruster operating conditions.[1]

III. Description of Modeling Study

A. Cathode Position and Mobility Study: Nine Case Matrix

There are two major goals in this study. The first is to evaluate how changing cathode position and the electron mobility inputs in HPHall affects the simulation results. The second is to create a HPHall simulation that closely matches actual thruster performance by choosing an appropriate cathode position and the electron mobility coefficient. Experimentally measured singly charged ion velocity is the basis of comparison for this combined study. At various locations on the thruster exit plane and in the near-plume, two types of comparisons were made; the velocity distribution function and the most probable velocity. The global performance parameters of thrust, discharge current, and beam current were also compared between the simulation and actual performance data.

A key factor for obtaining accurate simulation results is the modeling of the ion acceleration mechanism. The internal potential profile must be accurately represented in acceleration channel region of the simulation domain. Also, the electron mobility must be modeled appropriately so that ionization will occur in the proper region of the acceleration channel, allowing ions to be accelerated through the correct potential gradient. In order to study the effects of cathode position and electron mobility, a matrix of nine simulation cases was studied, where each case used a different combination of cathode position and Bohm mobility coefficient.

Three locations were chosen for the cathode boundary; the far cathode, the mid cathode, and the near cathode positions. These were chosen in equal magnetic stream function value increments spaced from the exit plane. Figure 2 shows the locations of the three cathode positions used in this study. The anode boundary was placed on a magnetic stream line upstream of the acceleration region and was not changed between the different cases. Figure 2 also shows the location of the anode position used in the simulations. Attempts to use the actual physical anode location led to unstable thruster discharge current.

Three Bohm mobility coefficients were used in this study, 0.15, 0.30, and 0.50. Simulations with a lower value of K_B were investigated, but the results indicated that higher K_B produced more physical results.

The time step duration for the simulation was 5×10^{-8} s and a total of 150,000 time steps were run in order to obtain good statistical ion velocity distributions. Velocity distribution functions at locations on the exit plane and near-plume were compared with LIF measurements. In these cases doubly-charged ions were modeled, but charge-exchange collisions were not. The simulated vacuum background pressure was set to 2×10^{-5} Torr.

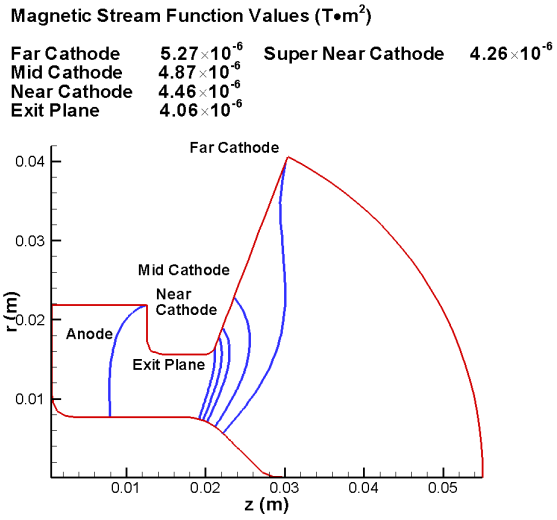

Figure 2. Magnetic streamlines of the three cathode positions and the exit plane.

B. Additional Cases

After the nine case matrix was studied, additional simulations were run in an attempt to simultaneously match global thruster performance parameters and ion velocity data. The input values chosen for the extra cases were derived from observations of the results of the nine case matrix, which will be

discussed in detail in Section V.

Thrust was most strongly affected by cathode position with the near cathode resulting in the highest thrust level. Discharge current was most strongly influenced by Bohm mobility coefficient. The low mobility coefficient, $K_B = 0.15$, resulted in discharge currents that most closely matched actual thruster performance. The most probable ion velocities of near cathode cases compared favorably with the LIF data at the exit plane. However, the ion velocity was too fast at points downstream of the exit plane because the effective discharge current was too high due to a large anode sheath term in the potential model which added additional potential to the inputted 250 V discharge potential.

Table 1. Additional Cases

New Case	Cathode Position	K_B Value	Discharge Voltage (V)
1	Super Near	0.15	250
2	Super Near	0.30	250
3	Super Near	0.30	235
3	Exit Plane	0.15	250
4	Exit Plane	0.30	250
5	Exit Plane	0.30	235

Six extra cases were run. Their input parameters are shown in Table 1. To match the performance data of the actual thruster, a higher thrust level was needed than any of the nine matrix cases provided. Two more cathode positions were used for the simulations: the super near cathode and the exit plane cathode. The super near cathode position was placed where the magnetic stream function had a value halfway between the value at the exit plane and the near cathode. The exit plane cathode was placed at the lambda line at the exit plane. It was predicted that the VDF shapes from the near cathode case would be preserved in the two new cathode positions. In order to keep the discharge voltage at a reasonable level new cases used the low and mid K_B values of 0.15 and 0.30. Also cases were run with lower a discharge voltage input (235 V) to account for the computed anode sheath's added contribution to the effective discharge voltage in order to prevent the ion velocity from being too high downstream of the exit plane.

IV. LIF Measurements

The experimental measurements presented in this work were performed in Chamber 6 at the Air Force Research Laboratory (AFRL) Electric Propulsion Laboratory at Edwards AFB, CA and originally presented by Hargus and Charles.[4] A revised analysis of this LIF data was undertaken to extract velocity distributions and correct previous systematic errors. The LIF measurement of xenon ion velocities is described more fully elsewhere.[4,7]

Due to the relatively narrow line shape of the 834.68 nm xenon ion transition (∼600 Mhz) relative to the broad distributions of the near-plume LIF profiles, deconvolution is not strictly required to closely approximate xenon ion velocity distributions from the raw LIF data in the near-plume region of the BHT-200-X3.[8] Not performing the deconvolution introduces an uncertainty estimated to be less than 10%. This allows the presentation of less strenuously conditioned LIF data to provide a qualitative xenon velocity distribution, avoiding the noise inevitably amplified by the deconvolution process.[8]

Table 2. Nominal Thruster Operating Conditions.

Anode flow	840 μg/s (Xe)
Cathode flow	98 μg/s (Xe)
Anode potential	250 V
Anode current	0.83 A
Keeper current	0.5 A
Magnet current	1.0 A
Heater current	3.0 A

Previous attempts to compare experimental ion velocities with results of numerical simulations have encountered difficulties. For example, simulation efforts have usually reported mean velocities from the calculated local VDF. Experimental methods such as LIF are often limited by poor signal to noise ratios and are best suited to measure the most probable velocity, corresponding to the peak of the velocity distribution function. In the skewed, non-symmetric distributions measured in Hall thruster plumes, the most probable (e.g. peak signal) and statistical mean velocities differ. Depending on the shape

of the distribution, these two bulk measures of velocity can vary significantly. The advantage of using a single bulk velocity measure is that it allows for the succinct presentation of large data sets. However, this method discards the majority of the available information. Comparison of the velocity distribution determined by each method allows for the most meaningful comparison with minimum ambiguity.

V. Results and Discussion

A. Cathode Position and Electron Mobility Study

Global Thruster Parameters

The first comparison is made between the simulation and experimental thruster performance parameters. The time-averaged performance parameters measured for BHT-200-X3 are shown along with HPHall predictions for each simulation configuration in Table 3. In all simulations, the predicted thrust is less than the measured thrust. Thrust increases in the simulations when the cathode position is closer to the exit plane as well as with increasing K_B values. The near cathode, $K_B = 0.50$ case has a predicted thrust that is closest to the measured value. However, this case predicts a discharge current a factor of two higher than the measured value, indicating that the model has difficulty predicting the electron current.

As an example of typical results, thruster performance parameters are plotted as a function of time for the final 500 μs of the simulation in Fig. 3 for the mid cathode, $K_B = 0.30$ case. The simulated thruster exhibits significantly higher magnitude discharge current oscillations than seen during experimental operation of the thruster. Simulated discharge current oscillations are approximately ±40% of the mean discharge current. Experimental oscillations are typically about 15%.

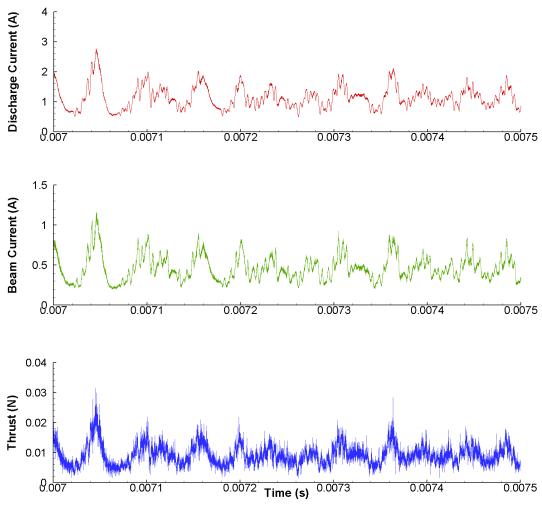

Figure 3. HPHall performance data during the last 500 μs of the simulation for the mid cathode, $K_B = 0.30$ case.

The best simulation agreement with regard to thrust generation is the near cathode, $K_B = 0.50$ case. The ion velocity flow field for this simulation domain is shown in Fig. 4. Ion acceleration begins at $z = 0.014$ m extending outward until at least 0.030 m, approximately 10 mm beyond the exit plane. The streamlines in Fig. 4 show a generally well focused near-field plume; however, there are some highly divergent streamlines near the outer diameter.

Figure 5 shows the effects of varying cathode position and K_B on the potential and Bohm cross-field mobility along the centerline of the acceleration channel. (Note that Bohm cross-field mobility is only calculated in the plasma acceleration region by HPHall and therefore is not shown on the plots outside of this region.) Figure 5(a) shows the potential and the cross-field mobility for the different cathode positions while K_B is kept constant at 0.30. A significant variation in potential profiles is observed among the different cathode positions. At the exit plane, the far cathode potential is about 15 V higher than the near cathode potential. This difference increases to approximately 70 V at 3 mm past the exit plane. This large variation in potential profile leads to significantly different ion velocity fields among the simulations with different cathode positions. Figure 5(a) also indicates that cross-field mobility is not strongly affected by cathode position, although there is some effect observed for the near cathode case at z values near the exit plane.

Figure 5(b) shows the effects of varying Bohm mobility coefficient while the cathode position is fixed at mid cathode position. It shows mobility increases linearly with increasing K_B value as described by Eqn. 2. The electron mobility affects the properties of the ionization region of the acceleration channel. Simulations with different electron mobility values will predict different near-field ion velocities due to the variation in the location of the ionization process. Figure 5(b) also shows a small change in the potential profile as a result of changing K_B. The profile is noticeably different for the $K_B = 0.15$ case than the other two cases.

Table 3. BHT-200-X3 performance data.

	Experimental		Far Cathode			Mid Cathode			Near Cathode		
		$K_B =$	**0.15**	**0.30**	**0.50**	**0.15**	**0.30**	**0.50**	**0.15**	**0.30**	**0.50**
I_D (A)	0.80[9]		0.635	1.02	1.40	0.720	1.15	1.61	0.788	1.33	1.93
I_B(A)	< 0.61		0.428	0.466	0.459	0.444	0.467	0.464	0.446	0.465	0.485
T (mN)	12		7.30	8.75	8.46	8.09	9.26	9.41	8.33	9.90	11.1

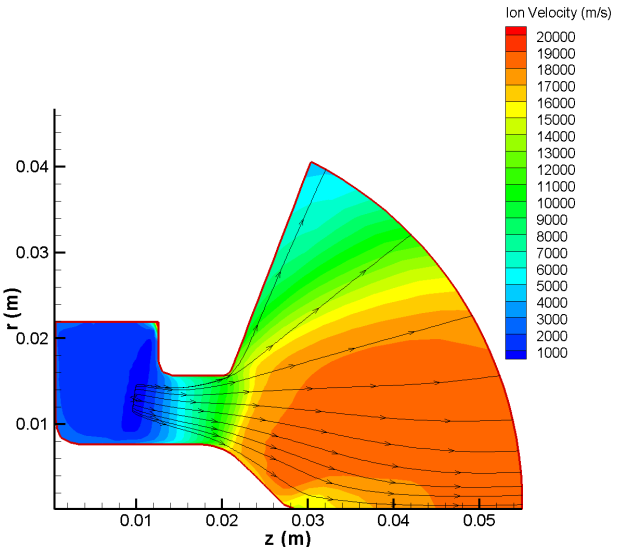

Figure 4. Ion velocity magnitude for the near cathode, $K_B = 0.50$ case. Ion velocity streamlines are shown to reveal the direction of the flow.

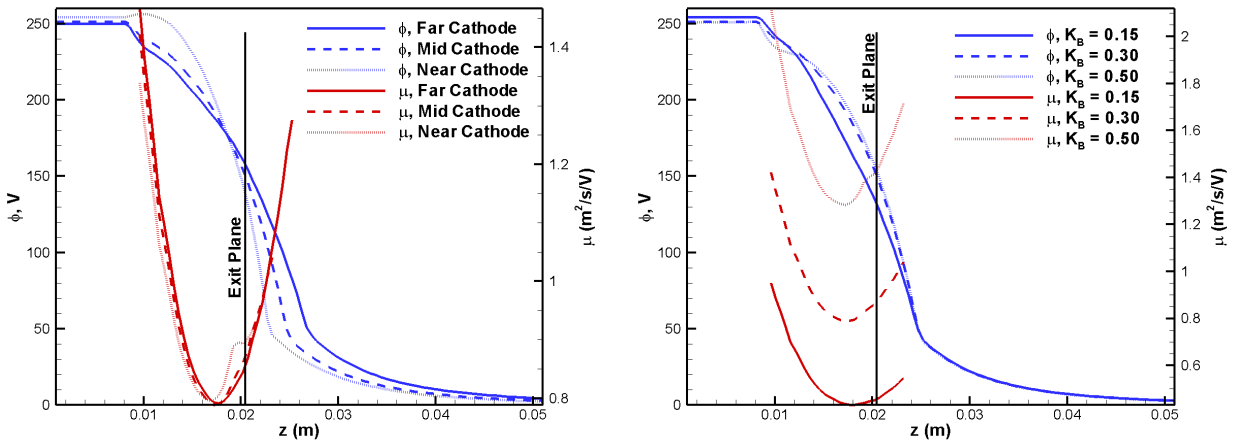

(a) Three different cathode positions, $K_B = 0.30$.

(b) Three different Bohm mobility coefficients, mid cathode position.

Figure 5. Potential and Bohm cross-field electron mobility along the channel centerline.

Bulk Velocity Comparisons

The simplest comparison between the LIF experimental data and the simulation results is the comparison of representative velocities. Immediately, the issue of which velocity best represents the flow may be raised. Numerically and with respect to global measures of performance such as thrust, the obvious choice would be the mean velocity. However, LIF measurements of velocity most clearly identify the peak of the velocity distribution. Signal noise and a variety of other issues produce significant uncertainties in determining the mean velocity from the LIF profiles, but the peak of the distribution is usually easily identified even in high noise environments. The velocity distribution peak represents the most probable velocity of the interrogated ions. The value of comparing the measured most probable velocities to those produced by the simulations is that it allows for large amounts of data to be compared quickly. However, as the flow complexity grows with distance from the exit plane due to convergence of the annular ion beam, the application of this comparison methodology fails when multiple ion populations mix.

Most probable axial and radial ion velocities along the centerline of the acceleration channel are plotted in Fig. 6. Axial velocity data shows how the ion acceleration differs between the simulations and the actual thruster. Radial velocity data provide a comparison of the beam focus. Large variations are observed among axial velocities of the simulations, especially within the first 10 mm downstream of the exit plane. The mid cathode, high mobility case exhibits erratic data due to dual peaks in its axial velocity distribution functions (seen in section A). For the most part, velocity increases at all axial locations as the cathode boundary is placed closer to the exit plane and as Bohm mobility is increased. The most notable difference between the simulations and the LIF data is the slope of the curve (i.e. the acceleration) within the first 10 mm downstream of the exit plane. All the simulation cases show that a larger portion of the ion acceleration occurs within this region than the LIF data indicate. The LIF data shows that the ions have reached 82% of their maximum velocity at the exit plane, whereas only 68% of the final velocity has been reached at the exit plane for the high mobility, near cathode case. Changes in the cathode boundary and the K_B value did not seem to significantly affect the slope of the velocity curve.

(fix most probable radial velocity data!)

Figure 7 displays the most probable ion velocities at the exit plane as a function of radial position. The experimental data show that the axial velocity is uniform at approximately 14.3 km/s and the radial velocity data is approximately symmetrically divergent about the center of the acceleration channel ($r = 0.012$ m).[4] Most simulations predict substantially lower axial ion velocities at the exit plane. As also observed in Fig. 6, the effect of cathode position on exit plane velocity is clearly visible as closer cathode positions result in an increase in most probable axial velocity. The electron mobility is also shown to increase exit plane axial velocity when the mobility is increased from low to mid value. However, when going from mid to high mobility, the axial velocity slightly decreases for the far cathode case and slightly increases for the near cathode case. Figure 7 also shows that neither the cathode position or the K_B value significantly affect the most probable radial ion velocity. All of the simulation radial velocities are slightly higher than the LIF data, but overall agreement is reasonable. The HPHall prediction of most probable axial velocity that has the best agreement with experimental data is the case with the near cathode position and the high K_B value of 0.50.

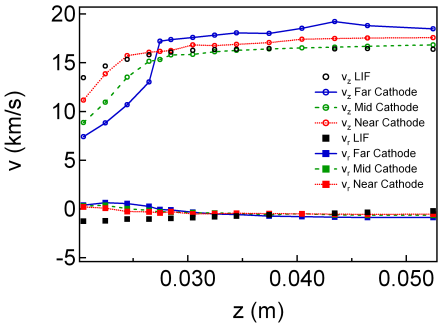

(a) $K_B = 0.15$.

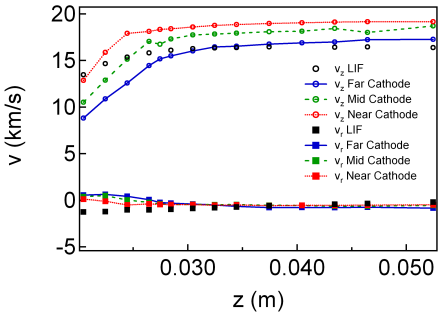

(b) $K_B = 0.30$.

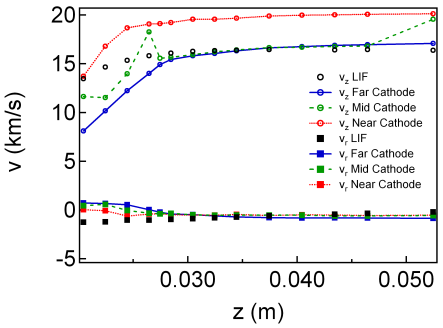

(c) $K_B = 0.50$.

Figure 6. Most probable ion velocity along the acceleration channel centerline ($r = 0.012$).

Figure 8 presents four types of data for each simulation in the nine case matrix. Average axial ion velocity

over the length of the acceleration channel centerline is plotted along with LIF measurements of the most probable and the average ion velocity. For the LIF data, the most probable velocity is smoother than the average velocity and more clearly represents the trend, but was observed to differ from the average by over 2 km/s at some locations. The LIF average velocity data is a more appropriate comparison to the HPHall average velocity data, but due to the noise in the LIF signal the average velocity data contains more error. The potential profile is also plotted along the acceleration channel centerline. For comparison, an estimated experimental value for the potential profile was calculated using the most probable LIF ion velocity data. Also included in Fig. 8 are contour plots of electron density and ionization rate in the simulation domain. These two plots reveal the effects of the electron physics on the ionization and ion acceleration processes.

The layout of Fig. 8 depicts the trends of how the simulation results change with cathode position and Bohm mobility coefficient. However, the near cathode, high mobility case does not neatly fit the trends established by the other cases. The reason for this inconsistency is the extra effective discharge voltage that results from the anode sheath potential term. This term accounts for an almost 20 V increase in potential in the acceleration channel.

Average axial ion velocity increases with both increasing mobility and positioning the cathode boundary closer to the exit plane. However, when mobility increases from $K_B = 0.30$ to $K_B = 0.50$ there is not a noticeable difference in axial velocity, except in the near cathode case where there is extra potential due to the anode sheath.

The electron density in the ionization region appears to increase in an approximately linear fashion with increasing Bohm mobility coefficient. Electron density reaches its highest values in the near cathode case for a given K_B value. Electron density also increases as the cathode boundary is positioned closer to the exit plane. From the ionization rate plots, most of the ionization appears to take place around $z = 0.012$ m. This feature however does not apply to the near cathode, high mobility case. Here the ionization rate is highest around $z = 0.009$ m. The ionization region also exhibits a more narrow band of concentration. The location of ionization is an additional source of high average velocity ions besides the additional potential of this case. Almost all the ions are formed at the highest potential regions of the acceleration channel.

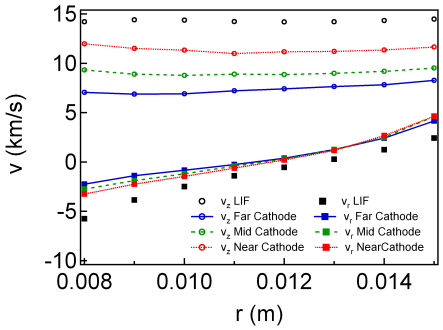

(a) $K_B = 0.15$.

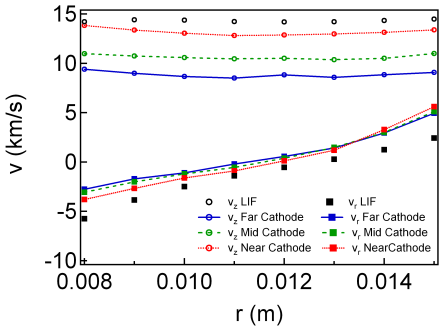

(b) $K_B = 0.30$.

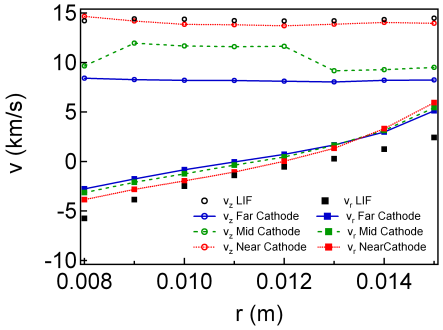

(c) $K_B = 0.50$.

Figure 7. Most probable ion velocity at the exit plane ($z = 0.020$ m) at various radial positions.

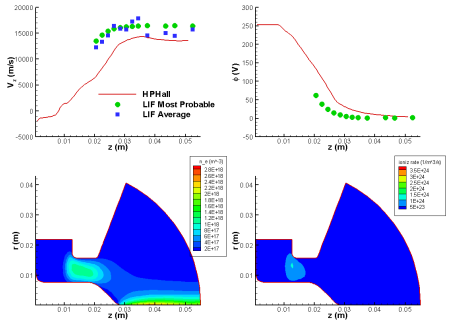

(a) Far Cathode, $K_B = 0.15$

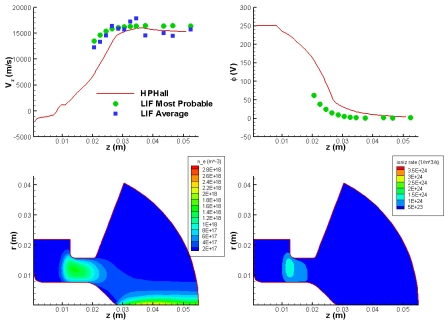

(b) Far Cathode, $K_B = 0.30$

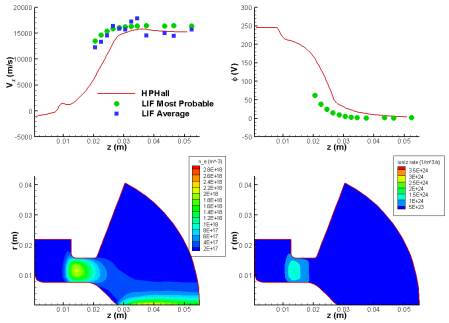

(c) Far Cathode, $K_B = 0.50$

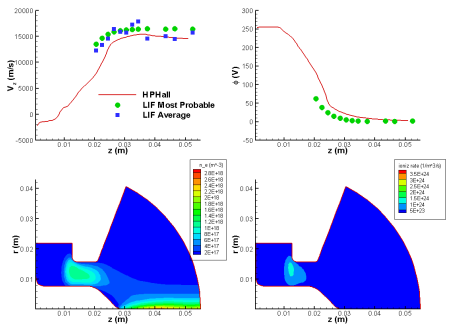

(d) Mid Cathode, $K_B = 0.15$

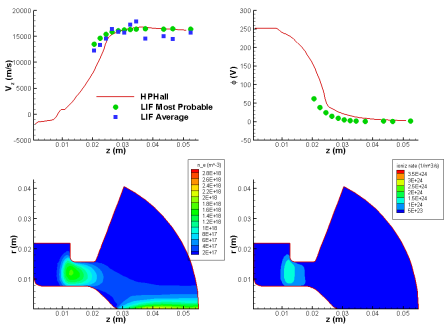

(e) Mid Cathode, $K_B = 0.30$

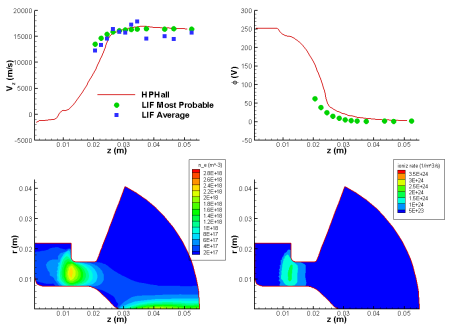

(f) Mid Cathode, $K_B = 0.50$

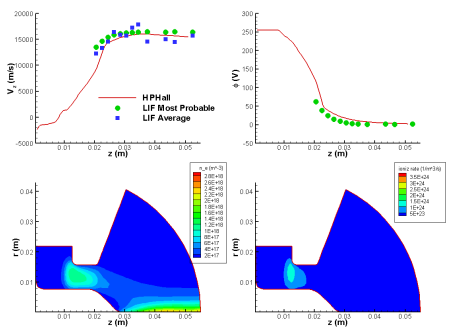

(g) Near Cathode, $K_B = 0.15$

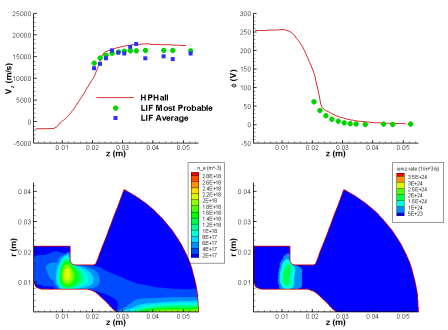

(h) Near Cathode, $K_B = 0.30$

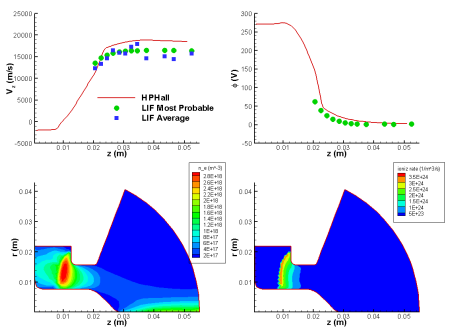

(i) Near Cathode, $K_B = 0.50$

Figure 8. Centerline axial velocity, centerline potential, electron density, and ionization rate for the nine case matrix

Ion Velocity Distributions

The limitations of comparing only most probable ion velocities is readily apparent in the small amount of information it conveys about the ions. It is therefore informative to compare the velocity distributions in various near-plume locations. It is assumed that if the simulations can predict near-plume ion distributions, then the internal physics are adequately captured.

Beginning with the centerline of the exit plane and extending in 10 mm increments in axial direction, we examine the evolution of the ion velocity distribution. For both measurement and simulations, ion velocity distribution functions at the center of the acceleration channel are shown in Figs. 11, 12, and 13 at the exit plane, and at distances of 10 and 20 mm beyond the exit plane. These plots show the effects of cathode position and K_B value on the evolution of velocity distribution. The best agreement with the axial data, in terms of distribution shape, appears with the near cathode placement when the two higher K_B values are used. At the exit plane, these cases predict velocities that are similar to the LIF data, but they over-predict velocity at the points beyond the exit plane. The radial velocity distributions are relatively insensitive to placement of cathode position and Bohm coefficient. All simulations have good overall agreement with the radial velocity LIF data at the exit plane and 10 mm past the exit plane. However, at 20 mm beyond the exit plane the simulations predict a larger portion of the flow having a negative radial velocity than the LIF data, indicating that the simulations predict over-focusing.

The Bohm coefficient strongly affects the width of the axial velocity distributions. The low $K_B = 0.15$ cross-field mobility coefficient tends to produce significantly broader distributions than the higher K_B values. At the $K_B = 0.30$ value, the mid cathode position simulation produces a double peaked axial velocity distribution. At present, the exact cause of this double peak is unknown. The value of K_B does not seem to have as dramatic of an effect on radial velocity distribution functions. However, various trends appear to be consistent for each cathode placement in the various simulations. For the near cathode case, increasing K_B results in narrowing radial velocity distributions. For the far cathode case, the opposite is true as increasing K_B appears to broaden the radial velocity distributions. These effects lessen further into the plume. The mid position cathode experiences little or no variation in radial velocity distributions although the axial distributions are quite different.

Exit plane velocity distributions near the inner insulator are important due to the proximity of the central magnetic pole. It is the erosion of the boron nitride cover of the central magnetic pole which limits thruster life. Figure 14 shows the velocity distributions determined by LIF measurement and the nine simulations. The measurements show that the axial velocity distribution here is different than that of the acceleration channel centerline. The familiar sharp peak is followed by a higher populated low velocity tail extending to zero velocity. Of the nine simulation cases, only the two higher Bohm conductivity, near cathode cases produce similar distributions to the measured data. All simulations under-predict the axial velocity here. The measured radial velocity distribution also exhibits a low velocity tail indicating that the flow in this region may be the result of several distinct ion populations. The simulations predict significantly less divergence than the measurements show. Also, the distinct low and reversed radial velocity feature is not captured. From the LIF data, it also appears than there may be a local source of ionization producing low velocity ions which are less well-collimated than the main peak due to the local divergence of the electric field.

Figure 15 shows the velocity distributions at the exit plane at a radial coordinate of 15 mm corresponding to a location near the outer insulator. The measured distributions are similar to that near the inner insulator shown in Fig. 14. This measured axial distribution has a sharper main peak than that of the inner insulator. The low velocity tail of the axial distribution is less pronounced and more uniform without local maxima. As in the previous exit plane cases, the simulation cases that best match the data are the near cathode, moderate and high Bohm conductivity cases. These simulations closely resemble the measured axial velocity distribution, but with a broader main peak. The measured radial velocity distribution is narrower than all the simulations. (Note that the flat top of the experimental radial distribution is an artifact due to signal saturation of the lock-in amplifier.) The simulated radial distributions are also significantly more divergent than the measured radial distribution. When taken in together, Figs. 14 and 15 show that the simulations under-predict the inward focus at the inner insulator wall and over-predict the plume divergence at the outer insulator.

Moving into the center of the near-plume, Fig. 16 shows the velocity distributions at 20 mm past the exit plane ($z = 0.040$ m) at $r = 2$ mm. Evidence of ion cross flow is observed, particularly in the radial velocity data where the flow from either side of the annulus can be clearly differentiated. The radial measurements also clearly show a distributed population of low velocity ions between the two radial velocity peaks. These

may be the result of momentum exchange collisions between the two ion streams. The general form of the axial distribution can be matched by the simulation, but not for cases with reasonable discharge currents. As in previous cases, it is not possible for the simulations to match both the magnitude and the shape of the axial distribution simultaneously. The agreement of the radial data is better. The simulations predict the peaks' shapes, but over-predict the velocity increment separation. This is indicative of the general simulation result incorrectly predicting radial flow divergence from the inner and outer portions of the anode annulus. The simulations predict a lower than measured intermediate radial velocity distribution. This may be a result of not modeling charge-exchange collisions or may indicate that the model does not predict the magnitude of plume ion collisions accurately. The discrepancy in the low radial velocity population may be due to an underestimation of the ion collision cross sections.

B. Additional Cases

Global Thruster Parameters

The global thrust parameters of the additional cases are displayed in Table 4. None of the new cases strongly matched both the experimental values of discharge current and thrust. Although both low mobility cases seem to the best attempts of this study. Once again the mid mobility cases significantly over-predict discharge current. The exit plane cathode, mid mobility case succeeds in predicting the correct thrust. However its prediction of discharge current is over a factor of two too high. For the super near cathode cases, both the low and mid mobility case only showed a small increase in thrust compared to the near cathode cases. Lowering the discharge voltage lowered the thrust, but did not significantly lower the discharge current.

Table 4. BHT-200-X3 performance data compared with new simulations.

Experimental			**Super Near Cathode**			**Exit Plane Cathode**		
		$K_B =$	0.15	0.30		0.15	0.30	
		$V_d =$	250 V	235 V	250 V	250 V	235 V	250 V
I_D (A)	0.80[9]		0.875	1.39	1.46	0.992	1.60	1.67
I_B(A)	< 0.61		0.455	0.464	0.473	0.459	0.475	0.490
T (mN)	12		8.97	9.92	10.7	9.80	11.0	12.0

Bulk Velocity Comparisons

Figure 10 shows the most probable axial ion velocities compared with LIF data. The super near cathode cases had velocities close to the measured values at the exit plane, but the velocities were too high by approximately 1 km/s downstream of the exit plane. All of the exit plane cathode cases greatly over-predicted axial velocity at all axial locations. The cases with a 235 V discharge displayed a lower velocity than the nominal discharge cases, but still were not close matching the experimental data.

Figure 9 shows the centerline velocity comparisons and electron properties for the additional simulations. In some cases, the average centerline velocity closely resembles the experimental most probable ion velocity. However, this comparison is not necessarily a good indication of correlation between the model and experimental data. Figure 10 clearly shows that the centerline most probable velocity from the model is greatly over-predicted. The super near cathode, low mobility case exhibits the best prediction of centerline potential.

Ion Velocity Distributions

Ion velocities at locations of interest are shown in Figs. 17, 17, 19, and 20. Figure 17 shows that axial VDF's for the super near cathode cases with mid mobility matched LIF velocity distributions well at the exit plane. However, the exit plane cathode cases all predicted axial velocities that were too great. Here the mid mobility cases produced distribution shapes that were similar to the LIF data. The low mobility cases produced distributions overly broad in shape.

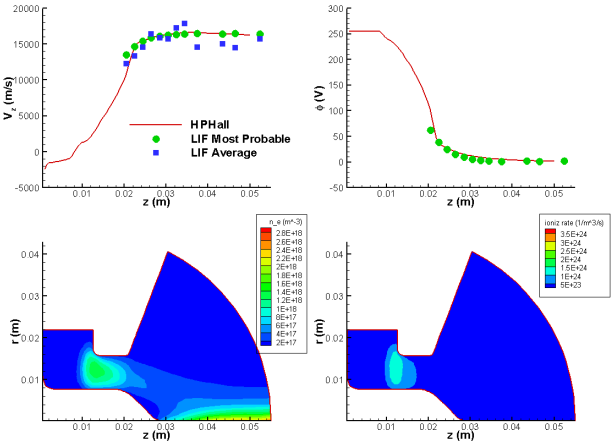

(a) Super Near Cathode, $K_B = 0.15$, Discharge Voltage = 250 V

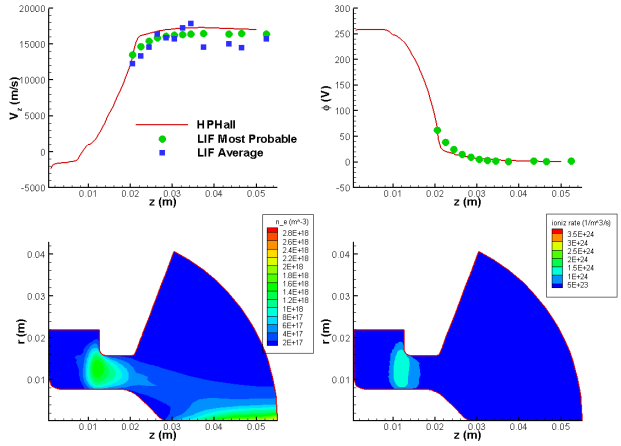

(b) Exit Plane Cathode, $K_B = 0.15$, Discharge Voltage = 250 V

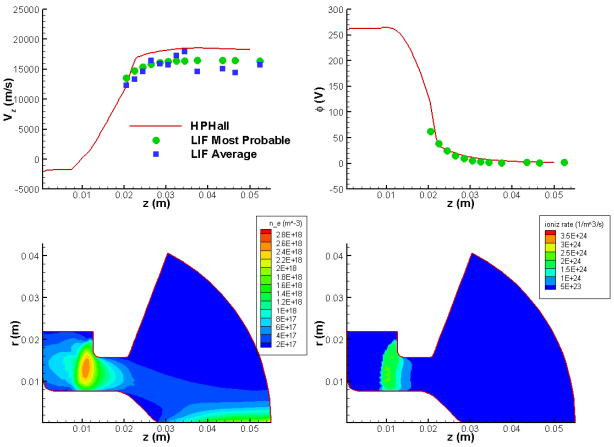

(c) Super Near Cathode, $K_B = 0.30$, Discharge Voltage = 250 V

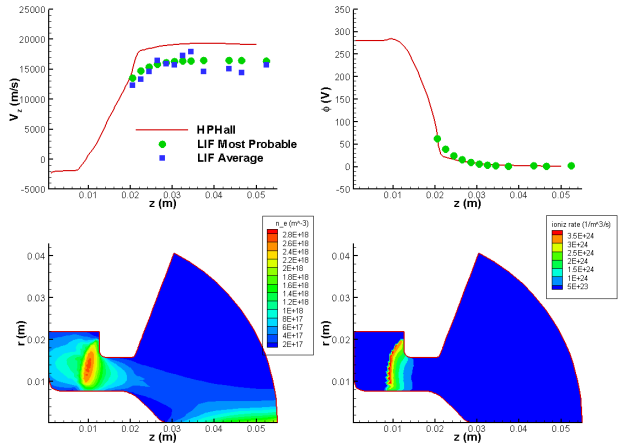

(d) Exit Plane Cathode, $K_B = 0.30$, Discharge Voltage = 250 V

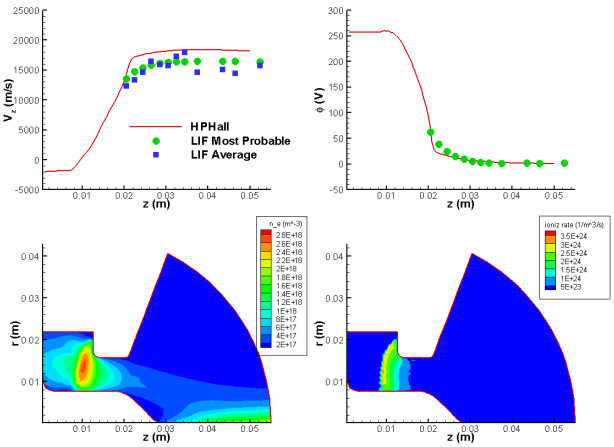

(e) Super Near Cathode, $K_B = 0.30$, Discharge Voltage = 235 V

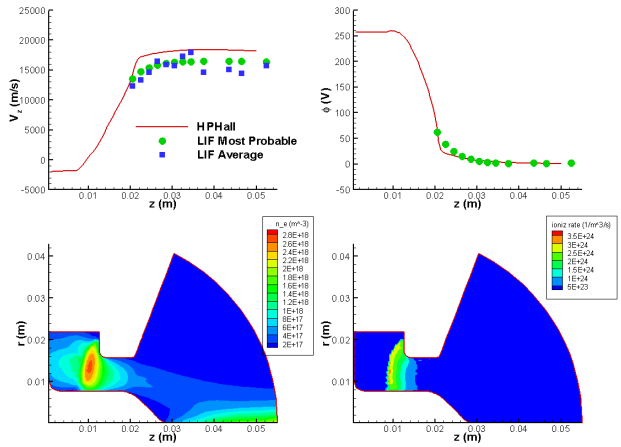

(f) Exit Plane Cathode, $K_B = 0.30$, Discharge Voltage = 235 V

Figure 9. Centerline axial velocity, centerline potential, electron density, and ionization rate for the new cases.

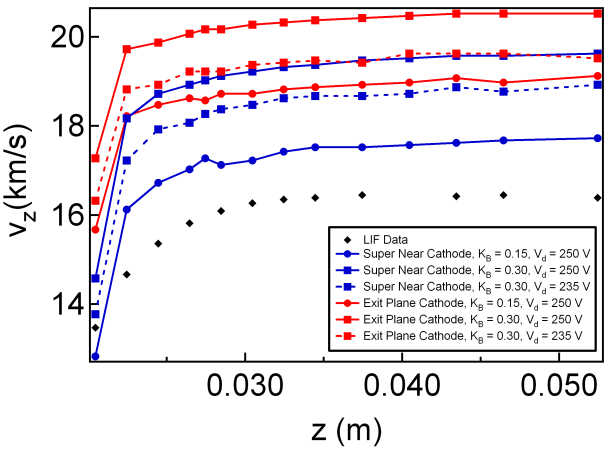

Figure 10. Most probable axial ion velocity along the acceleration channel centerline ($r = 0.012$ m)

Figures 17 and 19, 30 and 40 mm down stream of the exit plane on the acceleration channel centerline show similar trends. The axial velocities are over-predicted for all cases except the super near cathode, low mobility case. However the low mobility cases predict distributions that are too wide.

At the $z = 0.040$ m, $r = 0.012$ m location in the center of the near-plume the same phenomenon is observed as in the nine case matrix study. Figure 20 shows evidence of cross flow. The model again displays a slight over-focusing of the plume. The intermediate region of low-velocity ions between the peaks is once again not accounted for by the model.

VI. Conclusions and Future Work

Numerical simulation predictions from the HPHall code were compared to experimental ion velocity data. The simulations do not accurately predict the ion axial velocity magnitude or distribution functions consistently throughout the near-plume. Moreover, HPHall captures the trends but does not produce the discharge current and performance values obtained experimentally. The case with $K_B = 0.15$ and the near cathode boundary condition best matches the combination of discharge current and performance. However, the exit plane velocities are significantly lower than those measured and the velocity distributions in this case are significantly broader than that measured. Increasing values of K_B results in an improved correspondence of the velocity distributions; however, the simulations predict substantially higher final velocities than measured as well as unrealistically large discharge currents due to very high electron currents. None of the cathode boundary locations were able to match most probable axial velocity both at the exit plane and downstream. The near cathode boundary condition produced axial velocity data that matched exit plane LIF data, but over-predicted velocity downstream.

The simulations produce radial distributions that match the measured data better than the axial profiles. However, the simulations consistently predict greater divergence, particularly with the higher values of the K_B parameter. These cases with the higher K_B values have considerably larger discharge currents, and hence electron current, than actual thruster operation. This indicates that the cross-field electron conductivity is excessive and models the ionization and acceleration regions further into the plume than the $K_B = 0.15$ case. At the exit plane, the result is that the measured distribution has a greater inward focus, while the simulations are more outwardly divergent. In the intersecting radial flow region downstream of the central magnetic pole, the results show consistent shifts between the two peaks representing the flow originating from opposite sides of the annular anode discharge. It is noteworthy to draw attention to the intermediate low velocity radial populations between the two peaks. These are clear in the experimental data, but not seen in the simulation results. These could be collisional effects that are currently not modeled by the code. Alternatively, a portion of the measured low velocity distribution may be due to saturation of the fluorescence signal. Saturation of the axial LIF signal has been examined in the vicinity of the acceleration channel centerline several millimeters downstream and the LIF data has been found to be in the linear regime. With probe beam powers less than 4 mW, it is not believed that the signal is saturated. However, this possibility will be closely examined in a future study.

A major difficulty in conducting the comparison study between the model and the experimental data was that most of the common data locations for comparison existed outside of region of simulation domain where the electron fluid equations are solved (i.e. between the anode and cathode boundaries). Downstream of the cathode boundary, linear interpolation is used to find thermalized potential and electron temperature. Unfortunately, only a few of the data point locations used for comparison fell between the anode and cathode boundaries of simulation. This difficulty points to the need for velocity measurements made within the acceleration channel of the Hall thruster. Future LIF experiments will be performed on a specially modified thruster, which allows laser access into the acceleration channel, to measure internal velocity distribution

functions. Comparing data points inside the acceleration channel will give a better indication of the ability of the model to predict the ion acceleration physics.

It should be noted that the non-standard geometry of the BHT-200-X3 Hall thruster may be responsible for some of the lack of correspondence of the simulations with experimental data. HPHall was originally designed to model the SPT family of Hall thrusters. The BHT-200-X3 thruster geometry varies considerably from that of the SPT, particularly in the geometry of the anode. The BHT-200-X3 has a large plenum region designed to increase neutral residence time, which is lined with the magnetically permeable anode material.[3]

HPHall fixes anode position at a magnetic streamline. The position of the anode was not varied during this study. The results of varying the cathode location in the simulations strongly imply that anode location will also influence the computed flow parameters. One of the major discrepancies between the simulation and experimental data was the most probable axial velocity along the acceleration channel centerline within 10 mm of the exit plane as seen in Fig. 6. Placing the anode farther away from the exit plane and thus increasing the anode-cathode distance may result in a potential profile that is more similar to the actual thruster. This would lead to more acceleration before the exit plane and a velocity curve with a smaller slope. Matching the slope of the most probable axial velocity versus axial distance curve by changing the anode-cathode distance will be the first step in creating a simulation that predicts most probable axial velocity accurately throughout the near-plume in future modeling efforts.

It is apparent that further analysis of the sensitivity of HPHall to various input parameters as well as the electron conduction mechanisms are warranted. However, the issues may be better accomplished by a joint simulation and experimental effort that attempts to characterize the ionization, acceleration, and electron conductivity within the acceleration channel. Knowledge of these internal properties will allow for the correct selection of simulation boundary conditions and may lead to the modification of the model electron conductivity and ionization assumptions. The objective is to create an accurate model of the internal plasma parameters of the BHT-200-X3 Hall thruster that can be applied to other Hall thrusters. This capability coupled with an accurate erosion model could then be used to predict the lifetime of a thruster via simulation.

VII. Acknowledgments

The authors would like to thank Lubos Brieda and David Berger for their assistance with modifying the HPHall code, Justin Koo for his helpful discussions concerning the simulation results, and Jared Ekholm for his assistance in documenting this study. Thanks also go to Shannon Cheng and Felix Parra from MIT for their helpful instruction in operating HPHall.

References

[1]Fife, J. M., *Hybrid-PIC Modeling and Electrostatic Probe Survey of Hall Thrusters*, Ph.D. thesis, Massachusetts Institute of Technology, Cambridge, MA, 1998.

[2]Hargus, Jr., W. A., *Investigation of the Plasma Acceleration Mechanism Within a Coaxial Hall Thruster*, Ph.D. thesis, Stanford University, Stanford, CA, 2001.

[3]Hruby, V. J., Monheiser, J. M., and Pote, B. M., "Busek BHT-200-X3 Patent," United States Patent Number 6,150,764, November 21, 2000.

[4]Hargus, W. A. and Charles, C. S., "Near Exit Plane Velocity Field of a 200 W Hall Thruster," *39th Joint Propulsion Conference*, Huntsville, AL, 2003, AIAA 2003-5154.

[5]Ansoft Corporation, "Maxwell SV Software," http://www.ansoft.com/maxwellsv/.

[6]Chen, F. F., *Introduction to Plasma Physics and Controlled Fusion*, Plenum Press, New York, 2nd ed., 1984.

[7]Hargus, Jr., W. A. and Capelli, M. A., "Laser-Induced Fluorescence Measurements of Velocity within a Hall Discharge," *Applied Physics B*, Vol. 72, 2001, pp. 961–969.

[8]Hargus, Jr., W. A., "Evolution of the Ion Velocity Distribution in the Near Field of a 200 W Hall Thruster," *53rd JANNAF Propulsion Meeting*, Monterey, CA, 2005.

[9]Beal, B. E., Gallimore, A. D., Haas, J. M., and Hargus, Jr., W. A., "Plasma Properties in the Plume of a Hall Thruster Cluster," *Journal of Propulsion and Power*, Vol. 20, No. 6, November-December 2004, pp. 985–991.

A. Velocity Distribution Function Plots

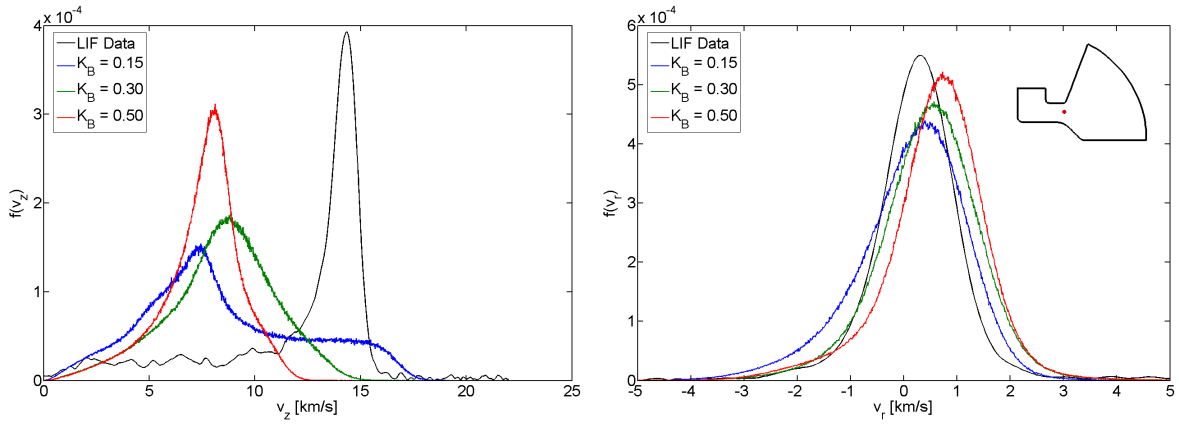

(a) $f(v_z)$, Far Cathode.

(b) $f(v_r)$, Far Cathode.

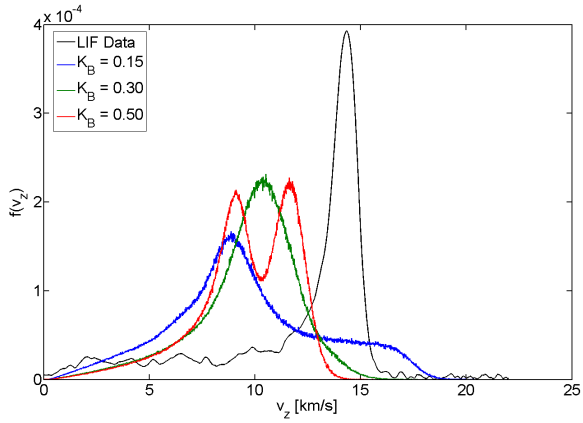

(c) $f(v_z)$, Mid Cathode.

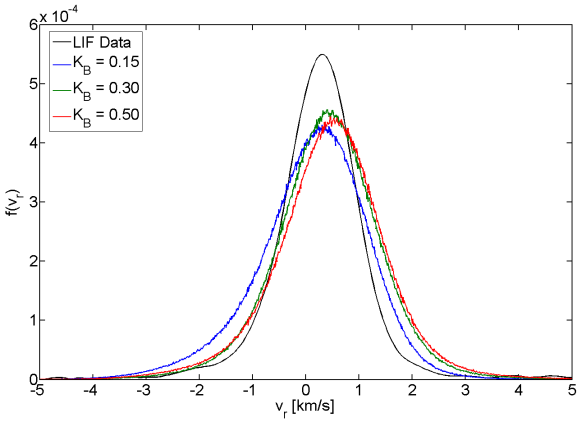

(d) $f(v_r)$, Mid Cathode.

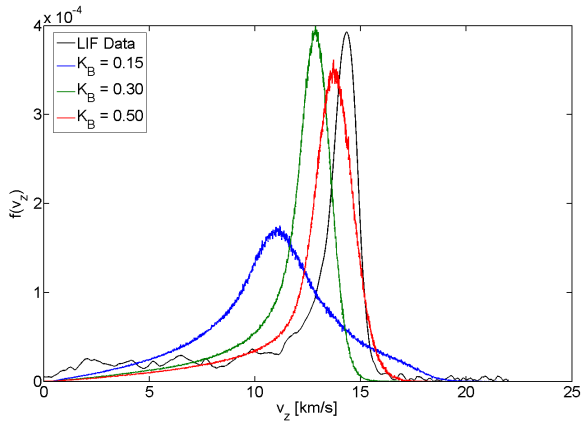

(e) $f(v_z)$, Near Cathode.

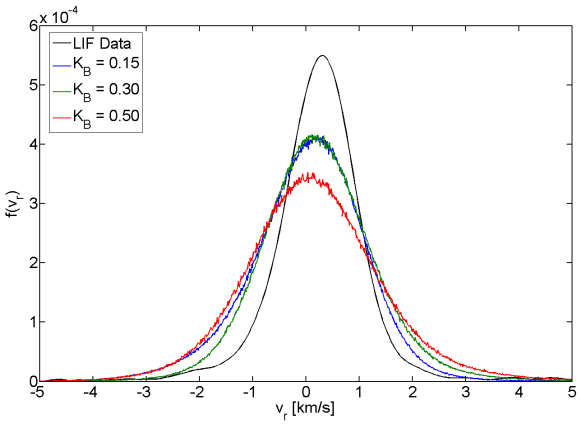

(f) $f(v_r)$, Near Cathode.

Figure 11. Ion velocity distribution functions at $z = 0.020$ m (exit plane), $r = 0.012$ m (channel center). Peaks are normalized by area.

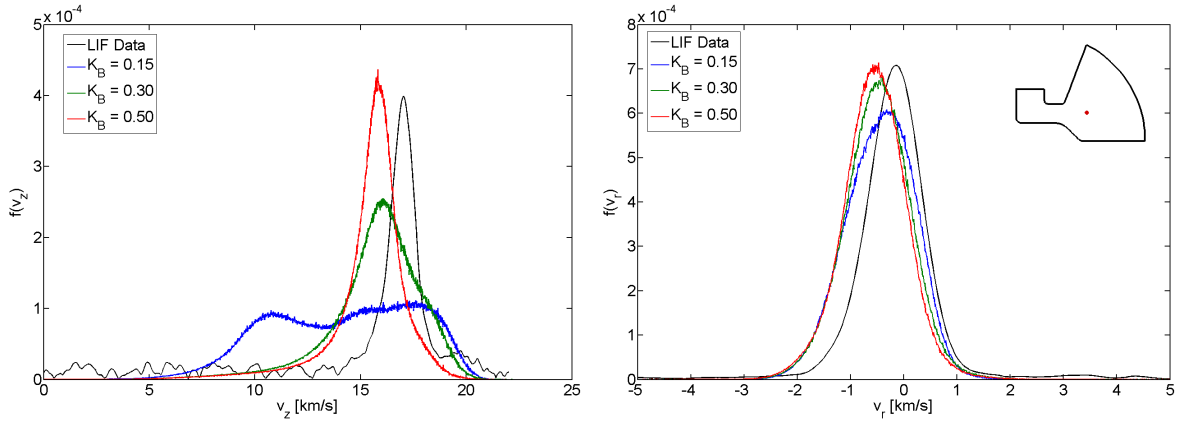

(a) $f(v_z)$, Far Cathode.

(b) $f(v_r)$, Far Cathode.

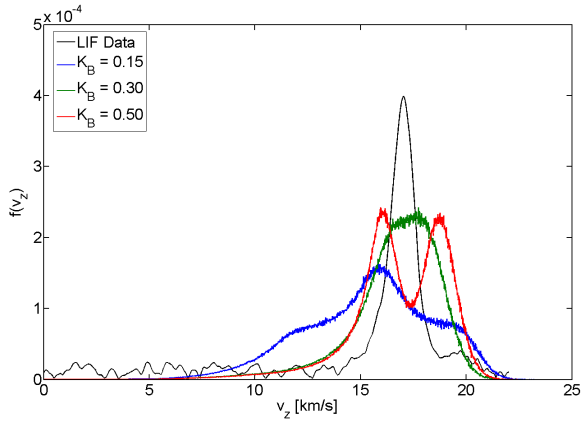

(c) $f(v_z)$, Mid Cathode.

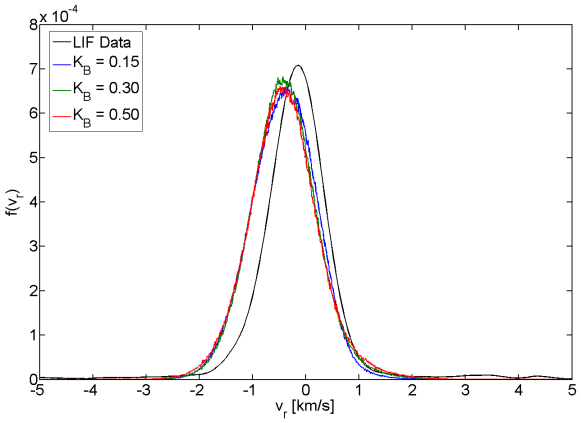

(d) $f(v_r)$, Mid Cathode.

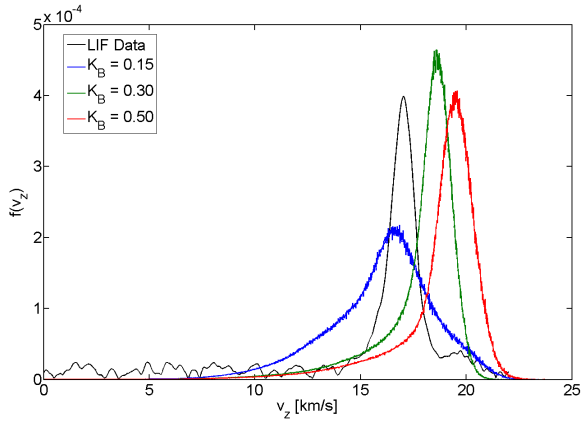

(e) $f(v_z)$, Near Cathode.

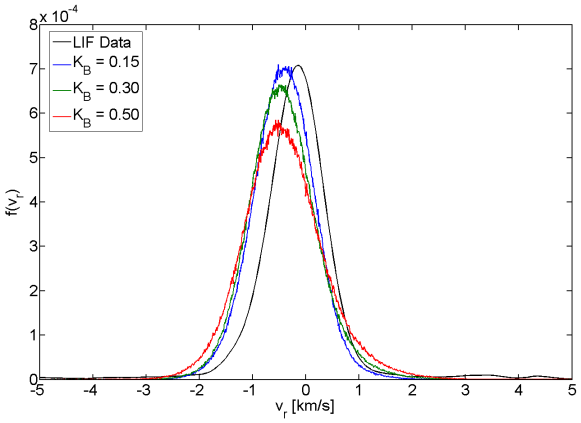

(f) $f(v_r)$, Near Cathode.

Figure 12. Ion velocity distribution functions at $z = 0.030$ m (10 mm past exit plane), $r = 0.012$ m (channel center). Peaks are normalized by area.

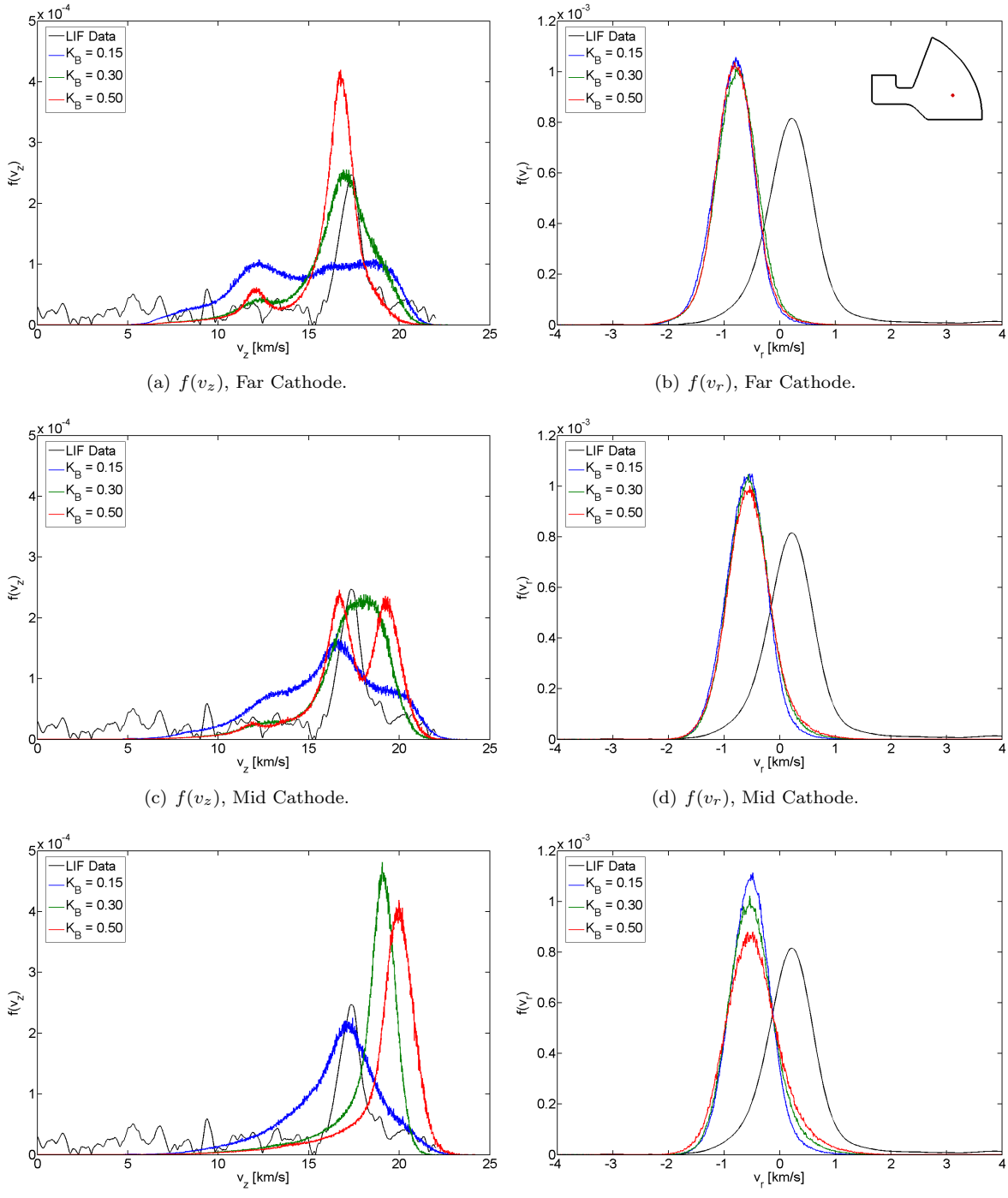

(a) $f(v_z)$, Far Cathode.

(b) $f(v_r)$, Far Cathode.

(c) $f(v_z)$, Mid Cathode.

(d) $f(v_r)$, Mid Cathode.

(e) $f(v_z)$, Near Cathode.

(f) $f(v_r)$, Near Cathode.

Figure 13. Ion velocity distribution functions at $z = 0.040$ m (20 mm past exit plane), $r = 0.012$ m (channel center). Peaks are normalized by area.

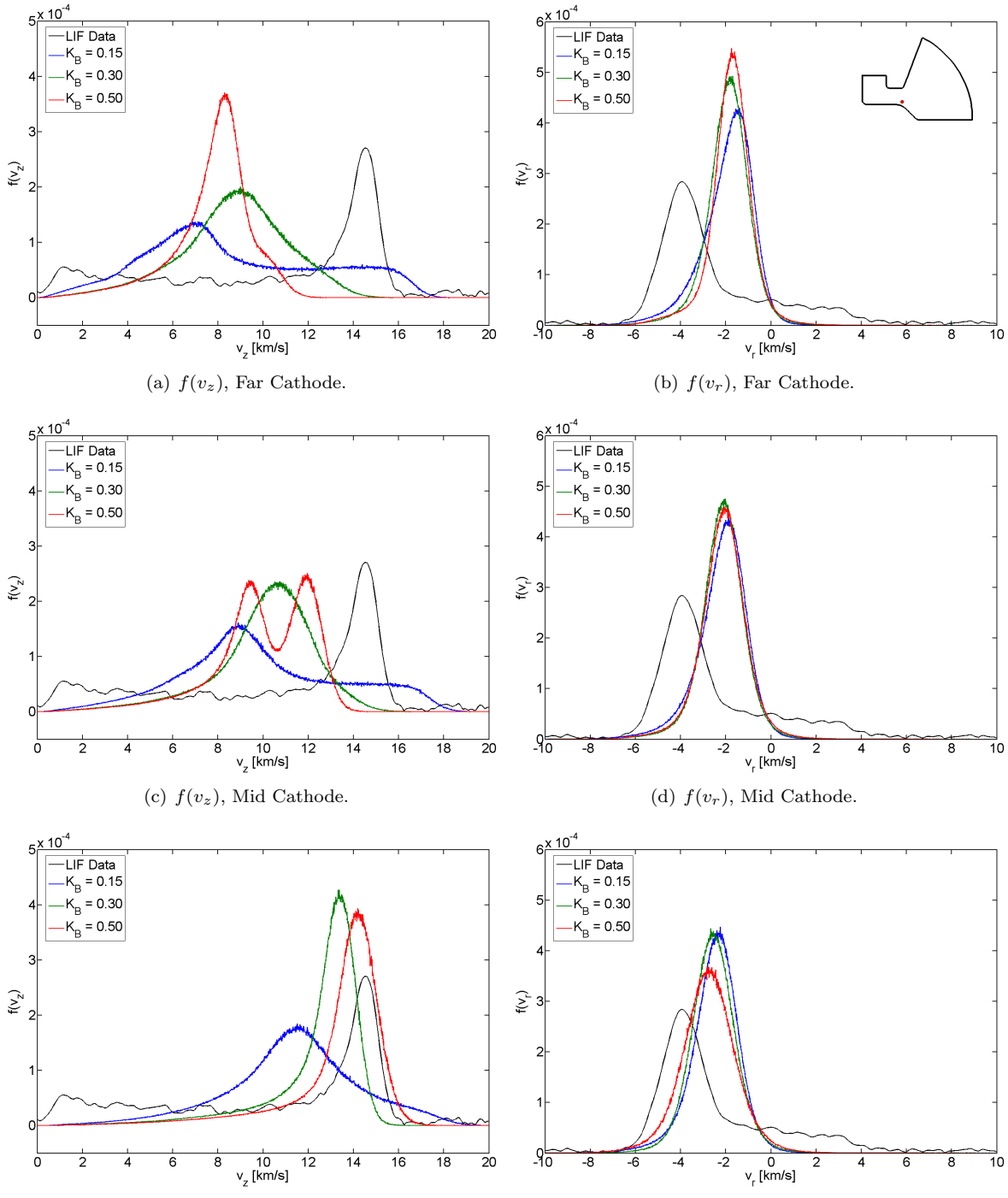

(a) $f(v_z)$, Far Cathode.

(b) $f(v_r)$, Far Cathode.

(c) $f(v_z)$, Mid Cathode.

(d) $f(v_r)$, Mid Cathode.

(e) $f(v_z)$, Near Cathode.

(f) $f(v_r)$, Near Cathode.

Figure 14. Ion velocity distribution functions at $z = 0.020$ m (exit plane), $r = 0.009$ m (near the inner insulator). Peaks are normalized by area.

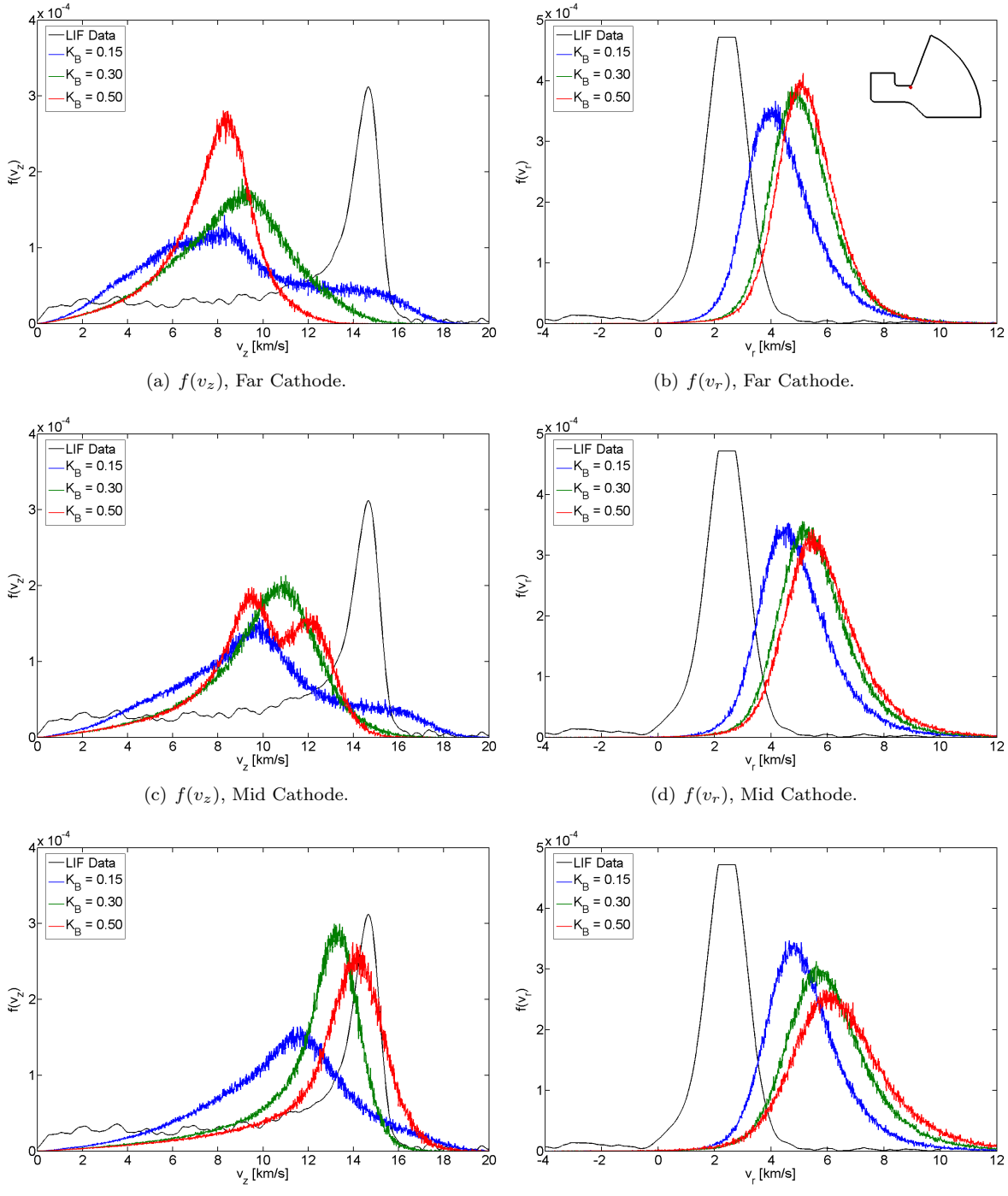

(a) $f(v_z)$, Far Cathode.

(b) $f(v_r)$, Far Cathode.

(c) $f(v_z)$, Mid Cathode.

(d) $f(v_r)$, Mid Cathode.

(e) $f(v_z)$, Near Cathode.

(f) $f(v_r)$, Near Cathode.

Figure 15. Ion velocity distribution functions at $z = 0.020$ m (exit plane), $r = 0.015$ m (near the outer insulator). Peaks are normalized by area.

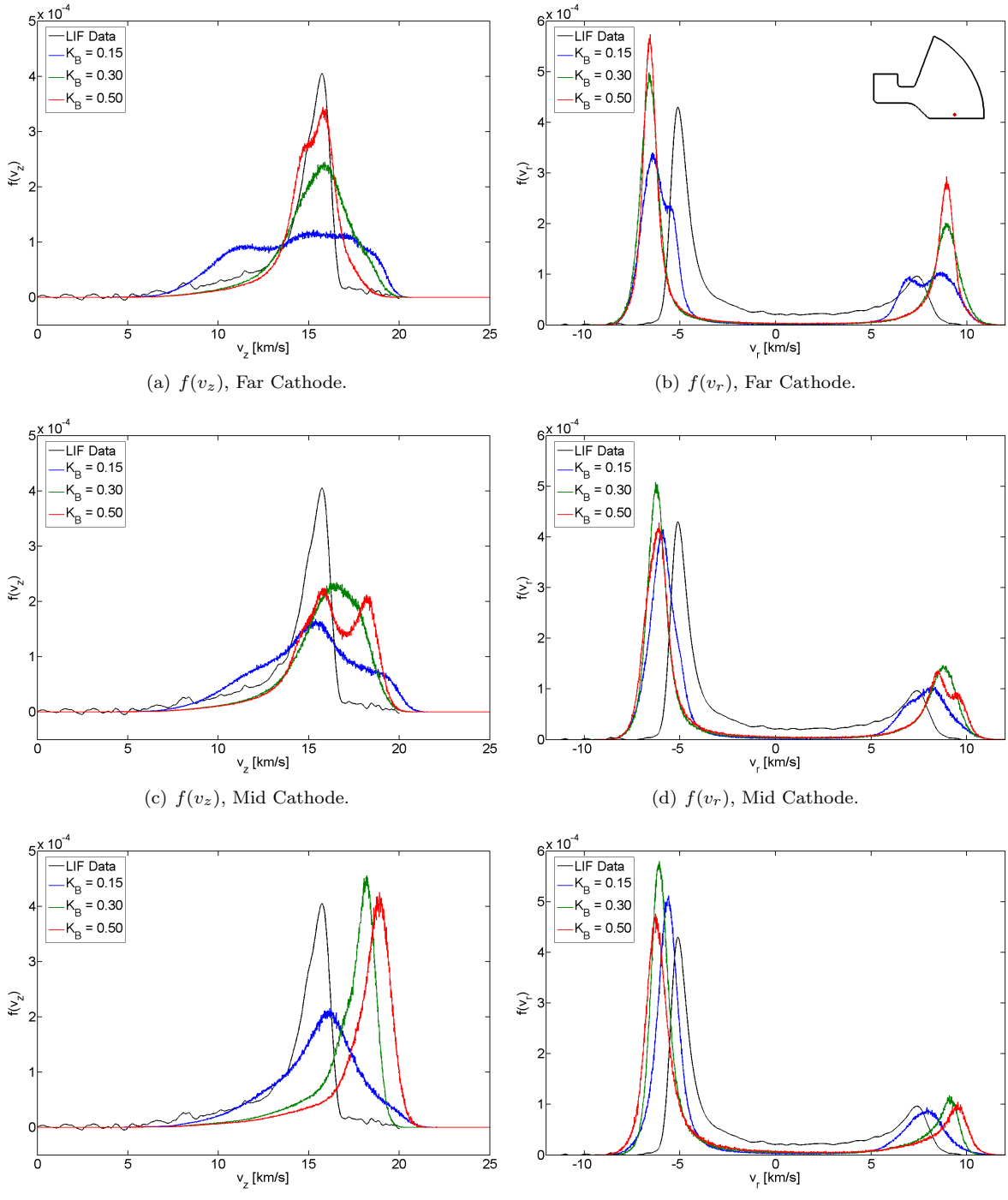

(a) $f(v_z)$, Far Cathode.

(b) $f(v_r)$, Far Cathode.

(c) $f(v_z)$, Mid Cathode.

(d) $f(v_r)$, Mid Cathode.

(e) $f(v_z)$, Near Cathode.

(f) $f(v_r)$, Near Cathode.

Figure 16. Ion velocity distribution functions at $z = 0.040$ m (20 mm past exit plane), $r = 0.002$ m (near the thruster centerline). Peaks are normalized by area.

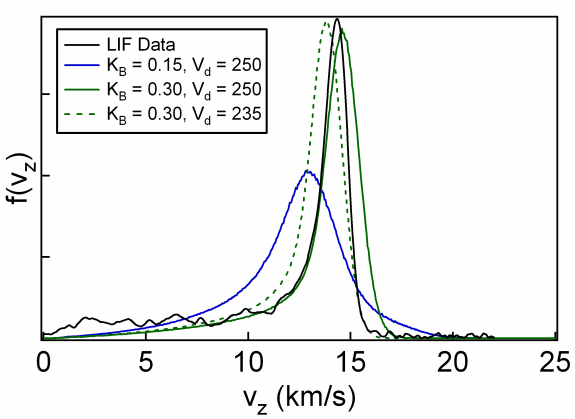

(a) $f(v_z)$, Super Near Cathode.

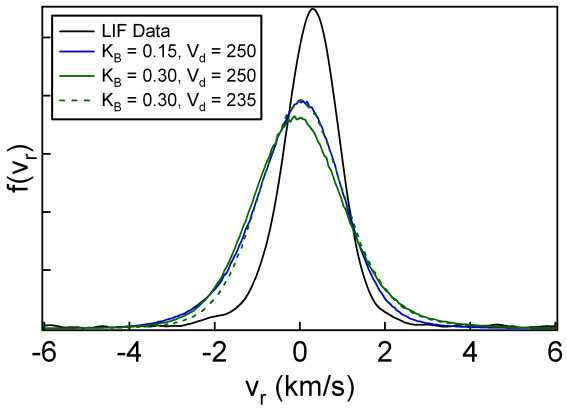

(b) $f(v_r)$, Super Near Cathode.

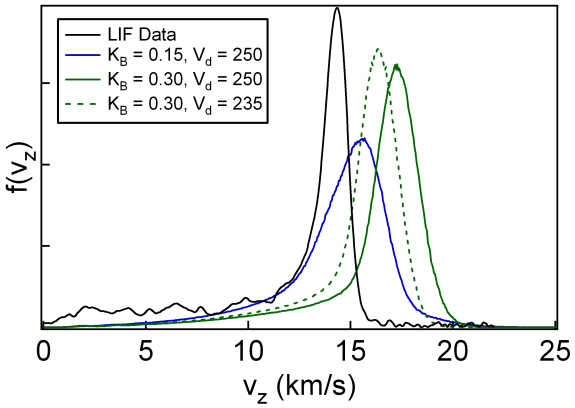

(c) $f(v_z)$, Exit Plane Cathode.

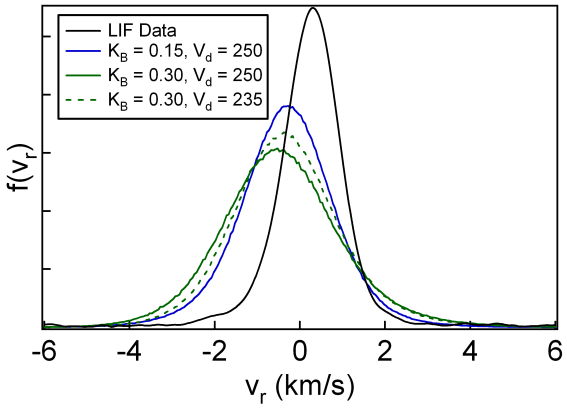

(d) $f(v_r)$, Exit Plane Cathode.

Figure 17. Ion velocity distribution functions at $z = 0.020$ m (exit plane), $r = 0.012$ m (channel center). Peaks are normalized by area.

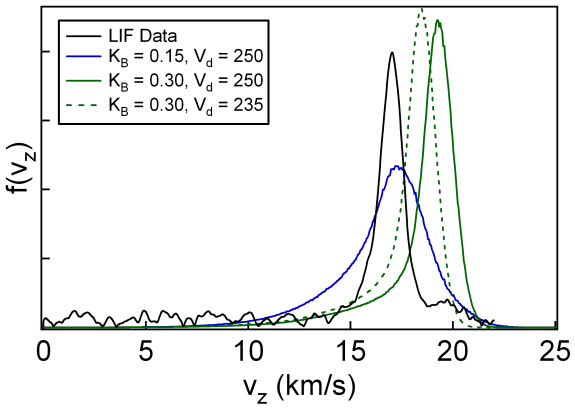

(a) $f(v_z)$, Super Near Cathode.

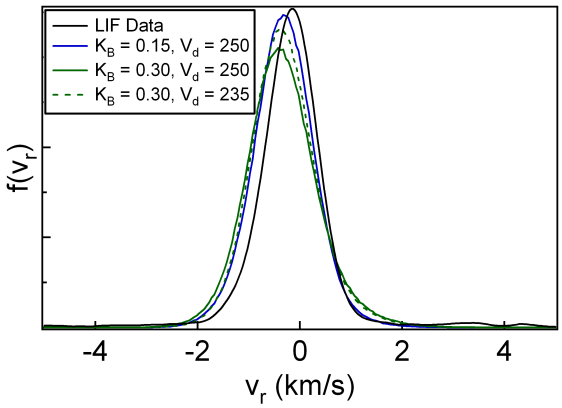

(b) $f(v_r)$, Super Near Cathode.

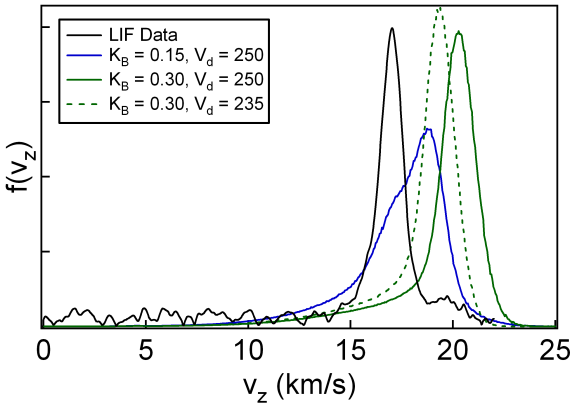

(c) $f(v_z)$, Exit Plane Cathode.

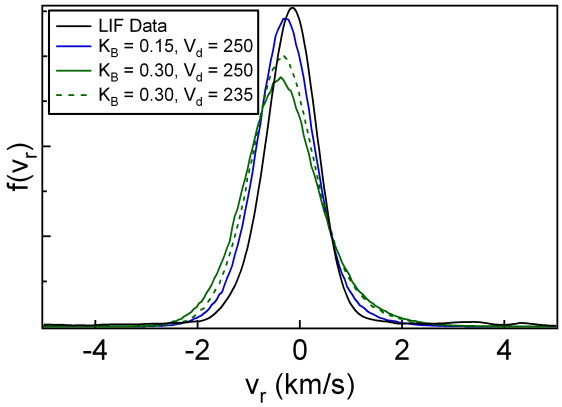

(d) $f(v_r)$, Exit Plane Cathode.

Figure 18. Ion velocity distribution functions at $z = 0.030$ m (10 mm past exit plane), $r = 0.012$ m (channel center). Peaks are normalized by area.

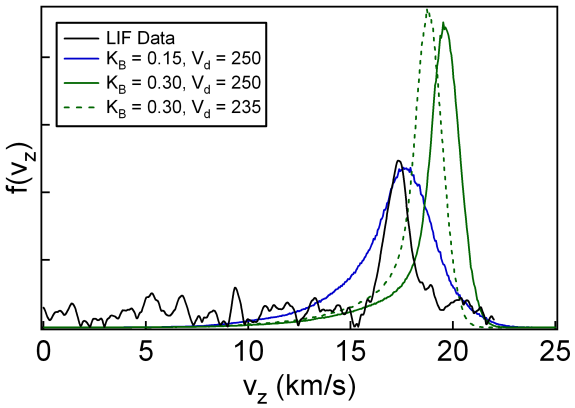

(a) $f(v_z)$, Super Near Cathode.

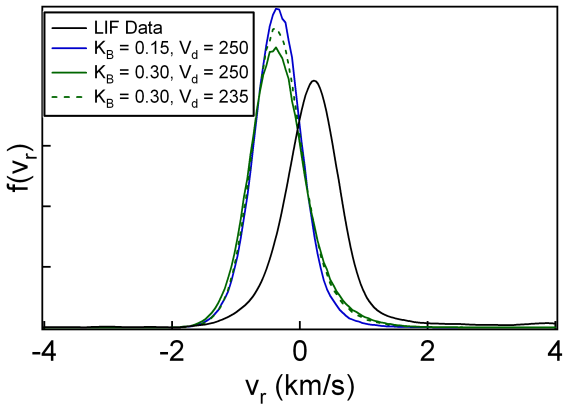

(b) $f(v_r)$, Super Near Cathode.

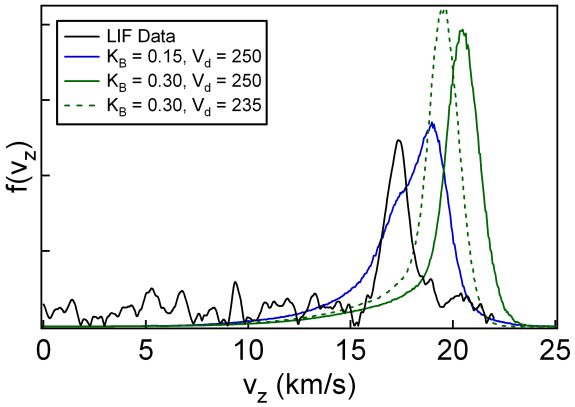

(c) $f(v_z)$, Exit Plane Cathode.

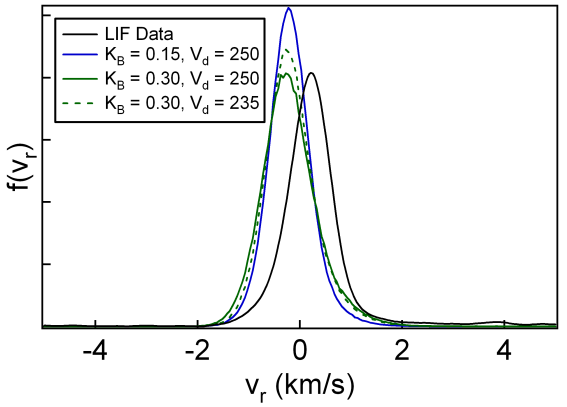

(d) $f(v_r)$, Exit Plane Cathode.

Figure 19. Ion velocity distribution functions at $z = 0.040$ m (20 mm past exit plane), $r = 0.012$ m (channel center). Peaks are normalized by area.

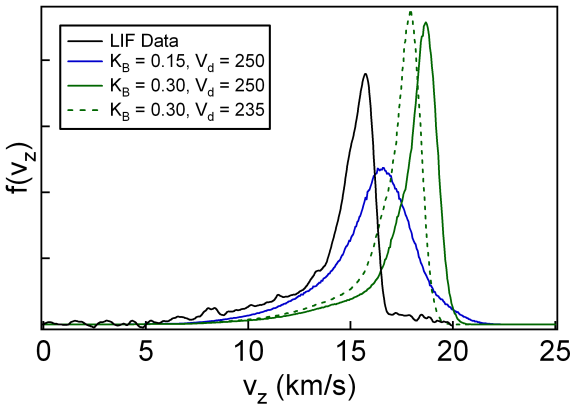

(a) $f(v_z)$, Super Near Cathode.

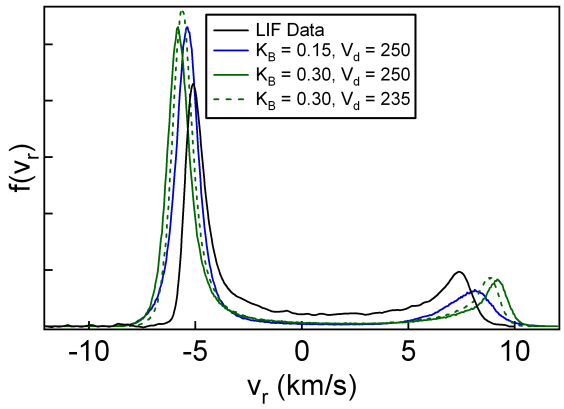

(b) $f(v_r)$, Super Near Cathode.

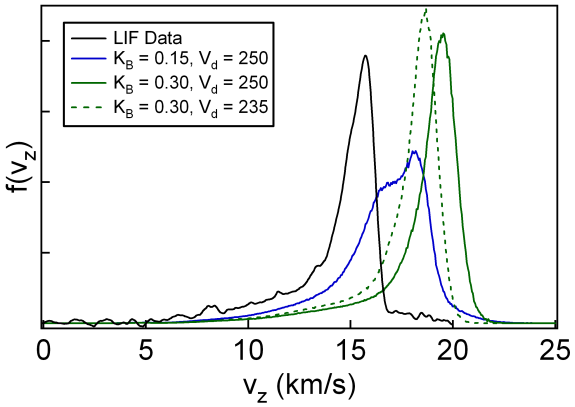

(c) $f(v_z)$, Exit Plane Cathode.

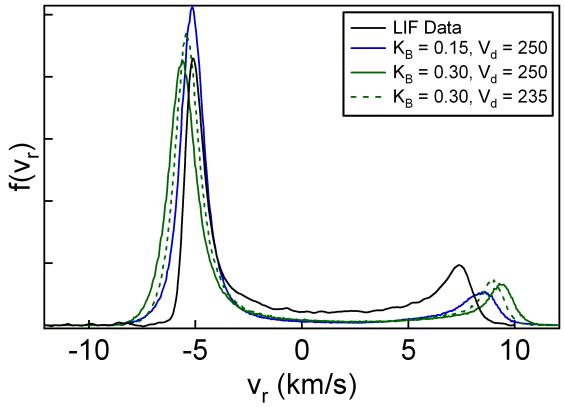

(d) $f(v_r)$, Exit Plane Cathode.

Figure 20. Ion velocity distribution functions at $z = 0.040$ m (20 mm past exit plane), $r = 0.002$ m (near the thruster centerline). Peaks are normalized by area.